

# The effects of bending on the resistance of elastically stretchable metal conductors, and a comparison with stretching

Cite as: Appl. Phys. Lett. **110**, 221906 (2017); <https://doi.org/10.1063/1.4984207>

Submitted: 26 February 2017 . Accepted: 13 May 2017 . Published Online: 01 June 2017

O. Graudejus , T. Li, J. Cheng, N. Keiper, R. D. Ponce Wong, A. B. Pak, and J. Abbas 



View Online



Export Citation



CrossMark

## ARTICLES YOU MAY BE INTERESTED IN

[Mechanisms of reversible stretchability of thin metal films on elastomeric substrates](#)

Applied Physics Letters **88**, 204103 (2006); <https://doi.org/10.1063/1.2201874>

[Stretchable gold conductors on elastomeric substrates](#)

Applied Physics Letters **82**, 2404 (2003); <https://doi.org/10.1063/1.1565683>

[Extended cyclic uniaxial loading of stretchable gold thin-films on elastomeric substrates](#)

Applied Physics Letters **94**, 071902 (2009); <https://doi.org/10.1063/1.3076103>

Lock-in Amplifiers  
up to 600 MHz



Watch



## The effects of bending on the resistance of elastically stretchable metal conductors, and a comparison with stretching

O. Graudejus,<sup>1,4,a)</sup> T. Li,<sup>2,a)</sup> J. Cheng,<sup>2</sup> N. Keiper,<sup>3</sup> R. D. Ponce Wong,<sup>4</sup> A. B. Pak,<sup>3</sup> and J. Abbas<sup>3</sup>

<sup>1</sup>*School of Molecular Science, Arizona State University, Tempe, Arizona 85287, USA*

<sup>2</sup>*Department of Mechanical Engineering, University of Maryland, College Park, Maryland 20742, USA*

<sup>3</sup>*Center for Adaptive Neural Systems, School of Biological and Health Systems Engineering, Arizona State University, Tempe, Arizona 85287, USA*

<sup>4</sup>*BioMedical Sustainable Elastic Electronic Devices (BMSEED) LLC, Center for Entrepreneurial Innovation (CEI), Phoenix, Arizona 85034, USA*

(Received 26 February 2017; accepted 13 May 2017; published online 1 June 2017)

Microcracked gold films on elastomeric substrates can function as stretchable and deformable interconnects and sensors. In response to stretch or deformation, the design would seek to minimize the change in resistance for stretchable or deformable interconnects; if used as resistive sensors, a large change in resistance would be desired. This research examines the change in resistance upon bending of a microcracked conductor and compares the results with stretching such a conductor. The resistance depends on the strain in the film, which, for bending, is a function of the bending radius and the location of the film within the structure with respect to the neutral plane. The resistance decreases when the gold conductor is under compression and increases when it is under tension. The decrease in resistance under compression is small compared to the increase in resistance under tension, marginally depending on the bending radius. In contrast, the resistance under tension significantly increases with decreasing bending radius. The mechanics model presented here offers a mechanistic understanding of these observations. These results provide guidance for the design of interconnects for flexible and stretchable electronics and for flexible sensors to monitor the magnitude and direction of bending or stretching. *Published by AIP Publishing.*

[<http://dx.doi.org/10.1063/1.4984207>]

Elastically stretchable thin films have potential applications as compliant interconnects,<sup>1,2</sup> soft electrodes in the biomedical field,<sup>3–6</sup> dielectric elastomer actuators,<sup>7</sup> and conformal sensors.<sup>8–10</sup> During utilization, these devices may be stretched and/or bent, each of which could affect the resistance of the stretchable film. It is therefore important to understand how bending and stretching affect the resistance of the stretchable film. For applications of stretchable conductors as interconnects, electrodes, and actuators, it is generally desirable for the resistance of the conductor to remain constant. For other applications, e.g., as resistive force, pressure, or bending sensors, it is desirable for the resistance to change significantly in order to achieve high sensitivity. This letter informs how to create device designs with the desired performance with respect to the change in electrical resistance.

Various technologies are suitable to fabricate stretchable conductors.<sup>11–14</sup> Microcracked gold films<sup>15,16</sup> on the elastomer polydimethylsiloxane (PDMS) are particularly well suited for commercial applications because these films can be produced, patterned, and encapsulated using standard microfabrication techniques.<sup>17,18</sup> Microcracked gold films form on PDMS during deposition at low temperatures (<65 °C) and at a gold thickness of 20–120 nm.<sup>16</sup> A thin layer of chromium or titanium (<6 nm) between the gold film and PDMS is used as an adhesion layer.<sup>16</sup> Previous research has examined the resistance vs. strain behavior by linearly or radially stretching the

conductor.<sup>19–21</sup> Under uniaxial tension, the resistance of the conductor increases with strain because (a) the geometry changes<sup>20</sup> as its length increases and its width decreases (Poisson compression), (b) the microcracks coalesce to form larger cracks (macrocracks),<sup>21</sup> and (c) the coalesced macrocracks become more densely and uniformly populated throughout the film. Poisson compression has two opposing effects on the conductor resistance. It causes the resistance to increase because of the reduction in the cross-section, and it causes the resistance to decrease because the compression bridges the microcracks. Due to the absence of Poisson compression in radial stretching, the resistance increase is significantly larger compared to uniaxial stretching.<sup>17,19</sup>

The energy release rate upon microcrack coalescence increases with the crack length (i.e., the larger cracks propagate preferentially) and decreases with the conductor width.<sup>21</sup> When the energy release rate for crack propagation exceeds the fracture toughness of the gold film, the crack propagates unstably across the entire width of the conductor and the resistance increases by several orders of magnitude.<sup>21</sup> Little is known about the behavior of these films under compression or bending. The major goals of this work are (1) to demonstrate that this microcracked gold film remains electrically conducting when a bending strain is applied, (2) to demonstrate that the normalized change in resistance is very different for bending compared to stretching for the same applied (stretching) or calculated (bending) strain, (3) to demonstrate the difference in behavior in compression and tension, previous research only looked at tensile strain during stretching,

<sup>a)</sup>Authors to whom correspondences should be addressed: oliver.graudejus@asu.edu and lit@umd.edu

and (4) to rationalize and explain the behavior upon bending with a mechanics model.

The tensile and compressive strain in a bent microcracked gold film depends on the distance of the film from the neutral plane,  $d_N$ , and the bending radius,  $BR$ . For a homogenous material, the strain  $\varepsilon$  is

$$\varepsilon = \frac{d_N}{BR}. \quad (1)$$

Figure 1(a) shows that the stress/strain curves of PDMS with and without a 57 nm thick Au film are nearly identical, i.e., the gold film does not have an appreciable effect on the mechanical properties of the PDMS (the elastic modulus is  $\approx 2$  MPa for each sample), thus substantiating the approach to treat the structure as homogenous. To investigate the effect of  $d_N$  and  $BR$  on the conductor resistance, the following structure was fabricated: PDMS substrate/Cr:Au conductor/PDMS encapsulation. The thickness of the PDMS substrate,  $d_S$ , was chosen to be 0.3 mm, 1.5 mm, or 3 mm. The 0.3 mm thick substrate was spin coated; the others were cast. The Cr:Au conductor (1 mm wide, 15 mm long, 3 nm Cr and 35 nm Au) was deposited through a shadow mask in a thermal evaporator (Edwards 306A). An electrical contact to the gold conductor was made with copper wires, mediated by silver paste. The PDMS encapsulation was cast in a Petri dish, and its thickness ( $d_E$ ) was chosen such that the overall thickness of the structure was 6 mm. Thus, structures were produced with the gold film at three different distances from the neutral plane: 2.7 mm ( $d_S = 0.3$  mm and  $d_E = 5.7$  mm), 1.5 mm ( $d_S = 1.5$  mm and  $d_E = 4.5$  mm), and 0 mm ( $d_S = 3$  mm and  $d_E = 3$  mm).

The resistance of each gold conductor was measured before, during, and after bending it along the curvature of cylinders with  $BR$  between 18 mm and 120 mm for 20 s. The conductors were in compression when the PDMS substrate was in contact with the cylinder and in tension when the conductor was flipped and the PDMS encapsulation was in contact with the cylinder, except for the sample in which the conductor was on the neutral plane. Figures 1(b) and 1(c) show the normalized change in resistance  $\Delta R/R_0$  (change in resistance  $\Delta R$  upon bending divided by the resistance before bending  $R_0$ ) for the three samples ( $d_N = 0$  mm, 1.5 mm, and 2.7 mm) as a function of  $BR$  [Fig. 1(b)] and  $d_N$  [Fig. 1(c)], both in compression and tension.

Under tension, the resistance of the gold conductor strongly increases with strain, i.e., the resistance is higher for smaller  $BR$  and larger  $d_N$  [Eq. (1)]. When the film is on the neutral plane ( $d_N = 0$  mm), bending should not induce strain and the resistance of the conductor is not expected to change. In our experiments, the resistance of conductors that were fabricated to have  $d_N = 0$  mm did change slightly ( $< 10\%$ ) for the smallest  $BR$  (highest strain), presumably because the conductor was located slightly off the neutral plane. It is experimentally challenging to place the conductor exactly on the neutral plane because even the slightest tilt in the sample during PDMS curing causes thickness non-uniformities. Additionally, the PDMS volume required for the encapsulation layer to achieve an overall sample thickness of 6 mm can only be approximated because it depends upon the volume of silver paste and the copper wires. Figure S1 (supplementary material)

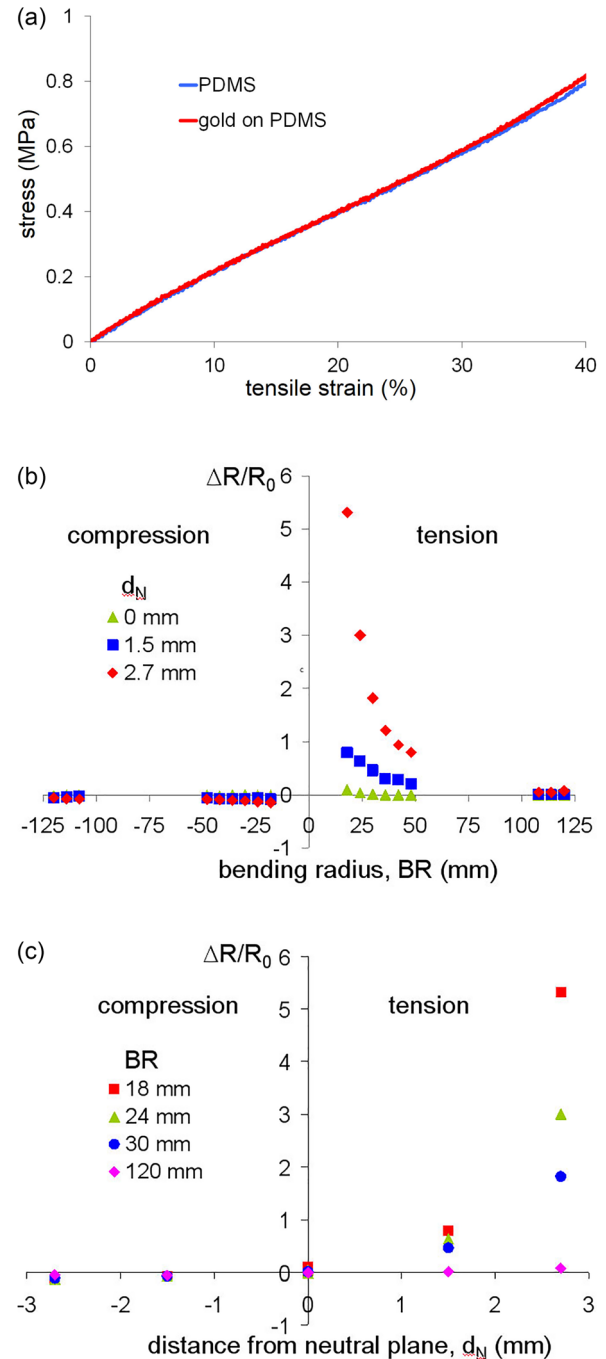


FIG. 1. (a) Stress-Strain curve for PDMS and a 57 nm thick microcracked gold film on PDMS, (b) normalized change in resistance ( $\Delta R/R_0$ ) vs. bending radius ( $BR$ ), and (c) normalized change in resistance ( $\Delta R/R_0$ ) vs. distance from the neutral plane ( $d_N$ ).

shows  $\Delta R/R_0$  values for several cycles of bending and relaxation, which were imposed manually. The increase in resistance is generally repeatable since a large portion of the observed cycle-to-cycle variability is likely due to variations in the degree of manual bending.

Under compression, the resistance of the gold conductor decreases with strain. For the same strain, the magnitude of the resistance decrease in compression is much smaller than the resistance increase in tension. For example, the resistance in compression decreases by 15% for the largest strain (largest  $d_N$ , smallest  $BR$ ) compared to an increase of over 500% ( $\Delta R/R_0 > 5$ ) in tension. The reason for this behavior is that

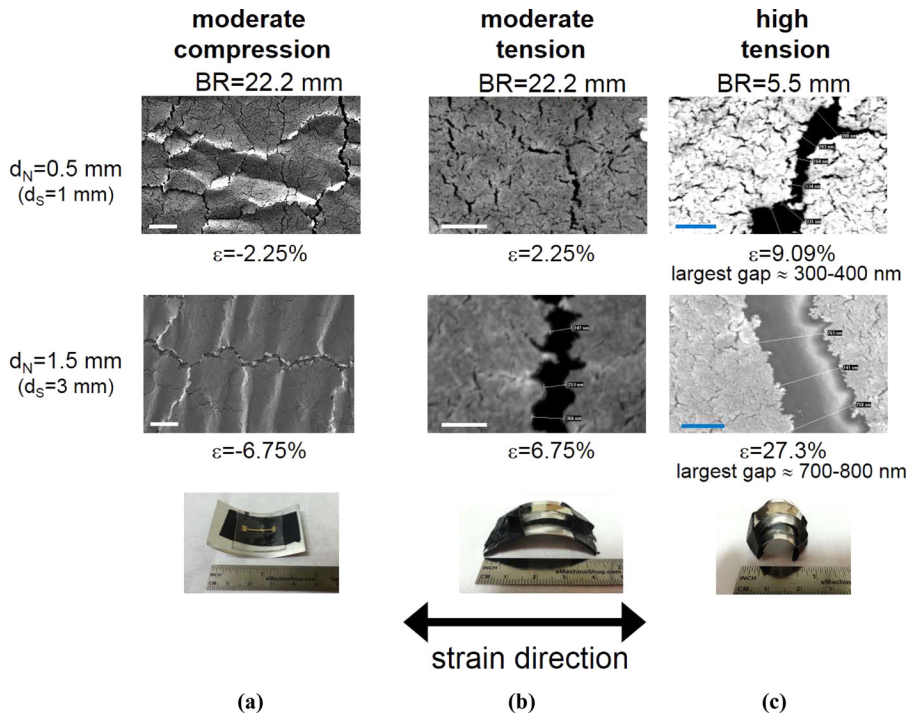


FIG. 2. SEM images of bent microcracked gold conductors at (a) moderate compression (scale bar:  $2\ \mu\text{m}$ ), (b) moderate, and (c) high tension (scale bar:  $500\ \text{nm}$ ).

the resistance of the conductor will only decrease when the microcracks are pushed together and the cracks close. The gaps in the microcracks are only a few tens of nanometers wide, and a small compressive strain is sufficient to bridge the gap. Once the gold on either side of the crack is in physical contact, further compression does not result in an additional decrease in resistance.

To investigate the effect of bending on the morphology of the gold film, scanning electron microscopy (SEM) images of bent (i.e., strained) gold films were obtained. To that end, we produced microcracked gold conductors on 1 mm and 3 mm thick PDMS substrates, i.e.,  $d_N = 0.5\ \text{mm}$  and  $1.5\ \text{mm}$ , respectively. The gold film was not encapsulated in order to facilitate SEM imaging. Figure S2 (supplementary material) shows that  $\Delta R/R_0$  values for encapsulated ( $25\ \mu\text{m}$  and  $150\ \mu\text{m}$  thick PDMS) and nonencapsulated gold conductors are comparable for strains up to 60%, which evidences that the coalescence of microcracks and the propagation of the resulting macrocracks are not appreciably affected by the presence of an encapsulation layer above the gold film.

Figure 2(a) shows SEM images of the bent gold film in moderate compression. The microcracks are pushed together in the direction of compression, causing the PDMS to buckle. However, cracks perpendicular to the direction of compression are not affected. Figures 2(b) and 2(c) show the SEM images of the gold film in moderate and high tension, respectively. As the strain increases, the microcracks coalesce to form larger cracks (macrocracks). The driving force for crack propagation increases with the crack length,<sup>21</sup> i.e., the larger microcracks propagate preferentially to form macrocracks. This is clearly evident from Figs. 2(b) and 2(c), where macrocracks are shown to be adjacent to microcracks. With increasing strain, the width of these existing macrocracks increases rather than additional microcracks coalescing to form macrocracks. For example, the width of the largest gap in a macrocrack increases from  $\approx 400\ \text{nm}$  at 9.09% strain

( $BR = 5.5\ \text{mm}$  and  $d_N = 0.5\ \text{mm}$ ) to  $\approx 800\ \text{nm}$  at 27.3% strain ( $BR = 5.5\ \text{mm}$  and  $d_N = 1.5\ \text{mm}$ ).

Figure 3 compares experimental data for the normalized change in resistance ( $\Delta R/R_0$ ) for bending and stretching of a microcracked gold conductor as a function of strain. The strain for the bending experiments ( $\epsilon_b$ ) was calculated according to Eq. (1), and the strain for the stretching experiments ( $\epsilon_s$ ) was calculated from the measured elongation ( $\epsilon_s = \Delta L/L_0$ ). The difference in  $\Delta R/R_0$  for bending and stretching also increases with strain. For example, at 15% strain, the resistance of a stretched conductor approximately doubles ( $\Delta R/R_0 \approx 1$ ), whereas the resistance of a bent conductor increases more than five-fold ( $\Delta R/R_0 > 5$ ). The reason for the reduced resistance increase for stretching is the Poisson compression in the conductor, which causes the lateral cracks to close up, thus reducing the resistance.<sup>22</sup> Poisson compression during bending is rather limited due to the geometric constraints.

Lower magnification SEM images of bent conductors [Fig. 4(a)] show that the distance between adjacent macrocracks decreases with strain, i.e., the macrocracks become denser and the macrocrack pattern becomes more uniform. In an effort to examine the role of the inter-crack spacing in the

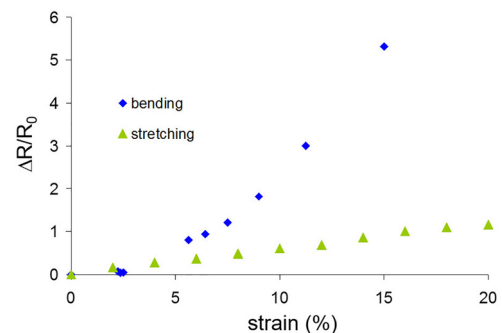


FIG. 3. Comparison of the normalized change in resistance ( $\Delta R/R_0$ ) vs. strain for bending and stretching a microcracked gold conductor.

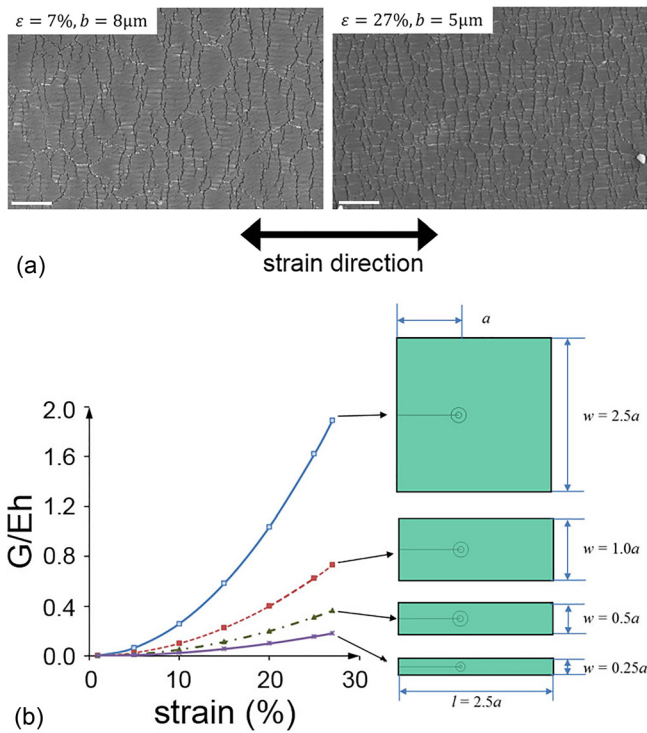


FIG. 4. (a) SEM image (magnification 800 $\times$ ) of macrocrack patterns and an average crack spacing of  $b = 8 \mu\text{m}$  at  $\varepsilon = 7\%$  and  $b = 5 \mu\text{m}$  at  $\varepsilon = 27\%$ , respectively (scale bar:  $20 \mu\text{m}$ ). (b) Normalized strain energy release rate  $G/Eh$  at different crack spacings.

crack growth process, we present a fracture mechanics model. In our simulation, a unit cell (with  $l \times w$  in dimension) representative of the microcracked gold film includes a single macrocrack of length  $a$  in the center [see Fig. 4(b)]. The width  $w$  of the unit cell represents the inter-macrocrack spacing  $b$ . To simplify the model, we treated the microcrack gold film material as homogeneous and isotropic with an effective Young's Modulus  $E$  and Poisson's ratio  $\nu$ . Such a simplification is common in fracture mechanics modeling.<sup>21,23–26</sup> The simulation is carried out using finite element code ABAQUS. A series of calculations was carried out to determine the strain energy release rate  $G$ , with a fixed value of  $l = 2.5a$  and  $w$  set to values of  $2.5a$ ,  $1.0a$ ,  $0.5a$ , and  $0.25a$  to mimic the decrease in inter-crack spacing. In all the four cases, the film was subject to a remote stretch loading up to the strain of 27%, which was the largest tensile loading applied in the experiments.

As shown in Fig. 4(b), the normalized strain energy release rate,  $G/Eh$  ( $h$  is the thickness of the gold film), of each crack increases with strain in the film; while at any given strain  $\varepsilon$ ,  $G/Eh$  is always higher for units with a larger  $w$ . This result indicates that those cracks located in the center of a wider film, or within an area where cracks are more sparsely distributed, have a larger driving force for crack advancing. Since the microcrack pattern obtained through deposition cannot be absolutely uniform, at the very first stage of a stretch, the initiation of crack advancing is random and leaves the film with nonuniformly dispersed macrocracks formed by microcrack coalescence. This creates a condition in which the film has irregular spacing of the macrocracks. Upon further stretch, microcracks preferentially advance in areas with larger macrocrack spacing due to the higher energy release rate. These macrocracks propagate

perpendicularly to the direction of tensile loading, which in turn reduces the macrocrack spacing. These processes repeat and generate a denser macrocrack pattern with more uniform crack spacing when the strain is high, as shown in the SEM images in Fig. 4(a).

We next developed a model to study the increase in electrical resistance of a cracked gold film with strain. The size of the representative cell is  $l \times w$  [Figs. 5(a)–5(c)], and in each cell, there are 6 macrocracks. The length of the cell  $l = 8a/3$ , where  $a = 30 \mu\text{m}$  is the length of each macrocrack, and the crack spacing in the length direction  $c = a/3$ . The width of the cell  $w = 3b$ , where  $b$  is the macrocrack spacing in the width direction for each of the cases studied [Fig. 4(a):  $b = 8 \mu\text{m}$  for  $\varepsilon = 7\%$ ;  $b = 5 \mu\text{m}$  for  $\varepsilon = 27\%$ ]. Then, a voltage was applied to the two sides of the representative cell after the cell was subject to the corresponding strain [Fig. 5(b)]. The governing equation for the electrical potential field is

$$\Delta U = 0, \quad (2)$$

where  $U$  is the applied voltage. This is mathematically identical to the steady state heat transfer problem, and thus, the

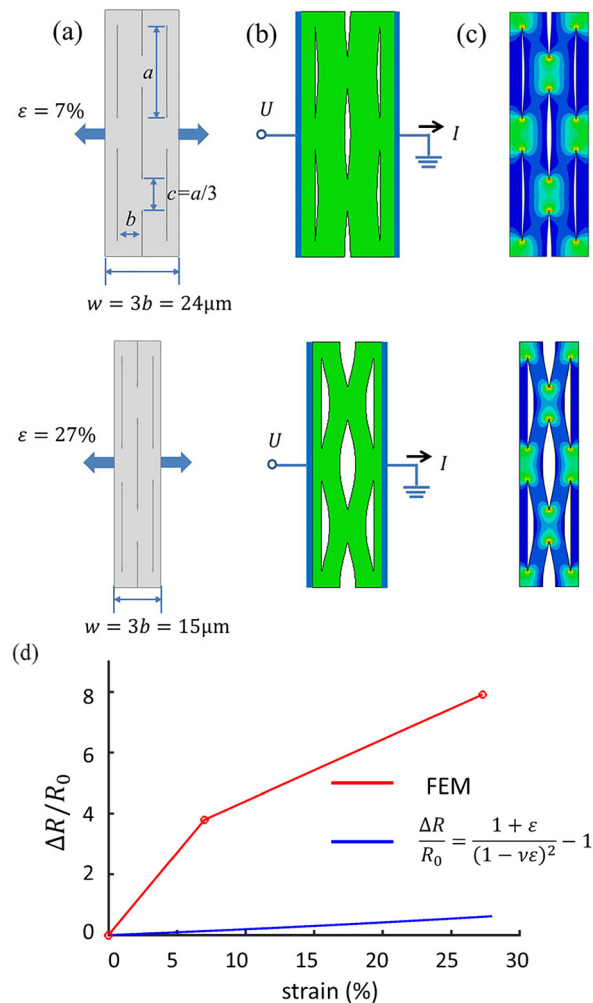


FIG. 5. Resistance of a gold film with macrocracks. (a) Schematics of the undeformed unit cell cut from the cracked gold film, with cell width  $w$  equals to  $3b = 24 \mu\text{m}$  for  $\varepsilon = 7\%$  and  $3b = 15 \mu\text{m}$  for  $\varepsilon = 27\%$ , and the number of macrocracks in each cell is 6, (b) deformed cell subject to voltage  $U$ , (c) horizontal component of the electrical field intensity, and (d) normalized change in resistance ( $\Delta R/R_0$ ) as a function of tensile strain.

boundary value problem (BVP) can be solved using the finite element method (FEM). Once the electrical potential field was solved, the effective resistance of the unit cell was calculated with the following equation:

$$R_{\text{eff}} = \frac{U}{\sigma \int E_x dA}, \quad (3)$$

where  $\sigma$  is the effective conductivity of the gold film,  $\mathbf{E} = \nabla U$  is the electrical field intensity, and  $dA$  is the area element of the unit cell boundary. The contour in Fig. 5(c) shows the magnitude of the component of  $\mathbf{E}$  along the direction of the established voltage (the  $x$  component) for each loading case. The resistance  $R_{\text{eff}}$  was normalized by the resistance of the undeformed (no macrocracks) counterpart of each unit cell  $R_0$  to produce a dimensionless representation. As shown in Fig. 5(d),  $\Delta R/R_0 = 3.8$  for  $\varepsilon = 7\%$  and  $\Delta R/R_0 = 7.9$  for  $\varepsilon = 27\%$ , i.e., the decrease in macrocrack-spacing upon applied tensile strain substantially alters the resistance of the film. These results obtained from the simulation accurately predict the resistance of the film upon bending. In contrast, analysis that only takes into account the changes in the conductor geometry upon bending<sup>20</sup> (i.e., using  $R = R_0(1 + \varepsilon)/(1 - \nu\varepsilon)^2$ ) fails to include the effects of microcrack coalescence and the decrease in macrocrack spacing on the resistance change.

In summary, the resistance of a microcracked gold conductor during bending is a function of the distance from the neutral plane and the bending radius. The increase in the resistance for bending is much larger than that for stretching at the same strain. This work will inform future designs for stretchable interconnects and sensors. For stretchable interconnects that may undergo bending, the goal is generally to minimize  $\Delta R/R_0$ , i.e., the gold film should be placed on or near the neutral plane. For stretchable sensors that may undergo bending, the goal is generally to maximize  $\Delta R/R_0$ , i.e., the gold film should be placed far from the neutral plane.

See [supplementary material](#) for the repeatability data on bending and a comparison of the normalized change in resistance for encapsulated and nonencapsulated gold conductors.

- <sup>1</sup>R. Carta, P. Jourand, B. Hermans, J. Thoné, D. Brosteaux, T. Vervust, F. Bossuyt, F. Axisa, J. Vanfleteren, and R. Puers, *Sens. Actuators, A* **156**, 79 (2009).
- <sup>2</sup>S. P. Lacour, J. Jones, S. Wagner, T. Li, and Z. Suo, *Proc. IEEE* **93**(8), 1459 (2005).
- <sup>3</sup>Z. Yu, O. Graudejus, C. Tsay, S. P. Lacour, S. Wagner, and B. Morrison III, *J. Neurotrauma* **26**(7), 1135 (2009).
- <sup>4</sup>K. W. Meacham, R. J. Giuly, L. Guo, S. Hochman, and S. P. DeWeerth, *Biomed. Microdevices* **10**(2), 259 (2008).
- <sup>5</sup>J. J. FitzGerald, S. P. Lacour, S. B. McMahon, and J. W. Fawcett, *IEEE Trans. Biomed. Eng.* **56**(5), 1524 (2009).
- <sup>6</sup>I. R. Mineev, P. Musienko, A. Hirsch, Q. Barraud, N. Wenger, E. M. Moraud, J. Gandar, M. Capogrosso, T. Milekovic, L. Asboth, R. F. Torres, N. Vachicouras, Q. Liu, N. Pavlova, S. Duis, A. Larmagnac, J. Vörös, S. Micera, Z. Suo, G. Courtine, and S. P. Lacour, *Science* **347**(6218), 159 (2015).
- <sup>7</sup>R. Pelrine, R. Kornbluh, and G. Kofod, *Adv. Mater.* **12**(16), 1223 (2000).
- <sup>8</sup>H. Vandeparre, D. Watson, and S. P. Lacour, *App. Phys. Lett.* **103**, 204103 (2013).
- <sup>9</sup>D. Qi, Z. Liu, M. Yu, Y. Liu, Y. Tang, J. Lv, Y. Li, J. Wei, B. Liedberg, Z. Yu, and Z. Chen, *Adv. Mat.* **27**, 3145 (2015).
- <sup>10</sup>O. Graudejus, Z. Yu, J. Jones, B. Morrison III, and S. Wagner, *J. Electrochem. Soc.* **156**(6), P85 (2009).
- <sup>11</sup>C. Zhou, S. Bette, and U. Schnakenberg, *Adv. Mater.* **27**(42), 6664 (2015).
- <sup>12</sup>J. A. Rogers, *Science* **327**, 1603 (2010).
- <sup>13</sup>M. Melzer, G. Lin, D. Makarov, and O. G. Schmidt, *Adv. Mat.* **24**, 6468 (2012).
- <sup>14</sup>Z. Song, T. Ma, T. Tang, Q. Cheng, X. Wang, D. Krishnaraju, R. Panat, C. K. Chan, H. Yu, and H. Jiang, *Nat. Commun.* **5**, 3140 (2014).
- <sup>15</sup>S. P. Lacour, D. Chan, S. Wagner, T. Li, and Z. Suo, *App. Phys. Lett.* **88**, 204103 (2006).
- <sup>16</sup>O. Graudejus, P. Goern, and S. Wagner, *Appl. Mater. Interfaces* **2**(7), 1927 (2010).
- <sup>17</sup>S. P. Lacour, S. Benmerah, E. Tarte, J. FitzGerald, J. Serra, S. McMahon, J. Fawcett, O. Graudejus, Z. Yu, and B. Morrison, *Medical & Biological Engineering Computation* **48**(10), 945 (2010).
- <sup>18</sup>O. Graudejus, B. Morrison, C. Goletiani, Z. Yu, and S. Wagner, *Adv. Funct. Mater.* **22**, 640 (2012).
- <sup>19</sup>T. Adrega and S. P. Lacour, *J. Micromech. Microeng.* **20**, 055025 (2010).
- <sup>20</sup>P. Mandlik, S. P. Lacour, J. W. Li, S. Y. Chou, and S. Wagner, *IEEE Electron Device Lett.* **27**(8), 650 (2006).
- <sup>21</sup>O. Graudejus, Z. Jia, T. Li, and S. Wagner, *Scr. Mater.* **66**, 919 (2012).
- <sup>22</sup>I. M. Graz, D. P. J. Cotton, and S. P. Lacour, *Appl. Phys. Lett.* **94**, 071902 (2009).
- <sup>23</sup>C. Peng, Z. Jia, D. Bianculli, T. Li, and J. Lou, *J. Appl. Phys.* **109**, 103530 (2011).
- <sup>24</sup>Z. Jia, C. Peng, J. Lou, and T. Li, *Thin Solid Films* **520**, 6576 (2012).
- <sup>25</sup>Z. Jia, M. B. Tucker, and T. Li, *Compos. Sci. Technol.* **71**, 365 (2011).
- <sup>26</sup>C. Peng, Z. Jia, H. Neilson, T. Li, and J. Lou, *Adv. Eng. Mater.* **15**, 250 (2013).

# **The Effects of Bending on the Resistance of Elastically Stretchable Metal Conductors, and a Comparison with Stretching**

**O. Graudejus<sup>1,4\*</sup>, T. Li<sup>2\*</sup>, J. Cheng<sup>2</sup>, N. Keiper<sup>3</sup>, R. Ponce Wong<sup>4</sup>, Adam B. Pak<sup>3</sup>, J. Abbas<sup>3</sup>**

*<sup>1</sup> School of Molecular Science, Arizona State University, Tempe, Arizona 85287, USA*

*<sup>2</sup> Department of Mechanical Engineering, University of Maryland, College Park, Maryland 20742,  
USA*

*<sup>3</sup> School of Biological and Health Systems Engineering, Arizona State University, Tempe, Arizona  
85287, USA*

*<sup>4</sup> BioMedical Sustainable Elastic Electronic Devices (BMSEED) LLC, Center for Entrepreneurial  
Innovation (CEI), Phoenix, Arizona 85034, USA*

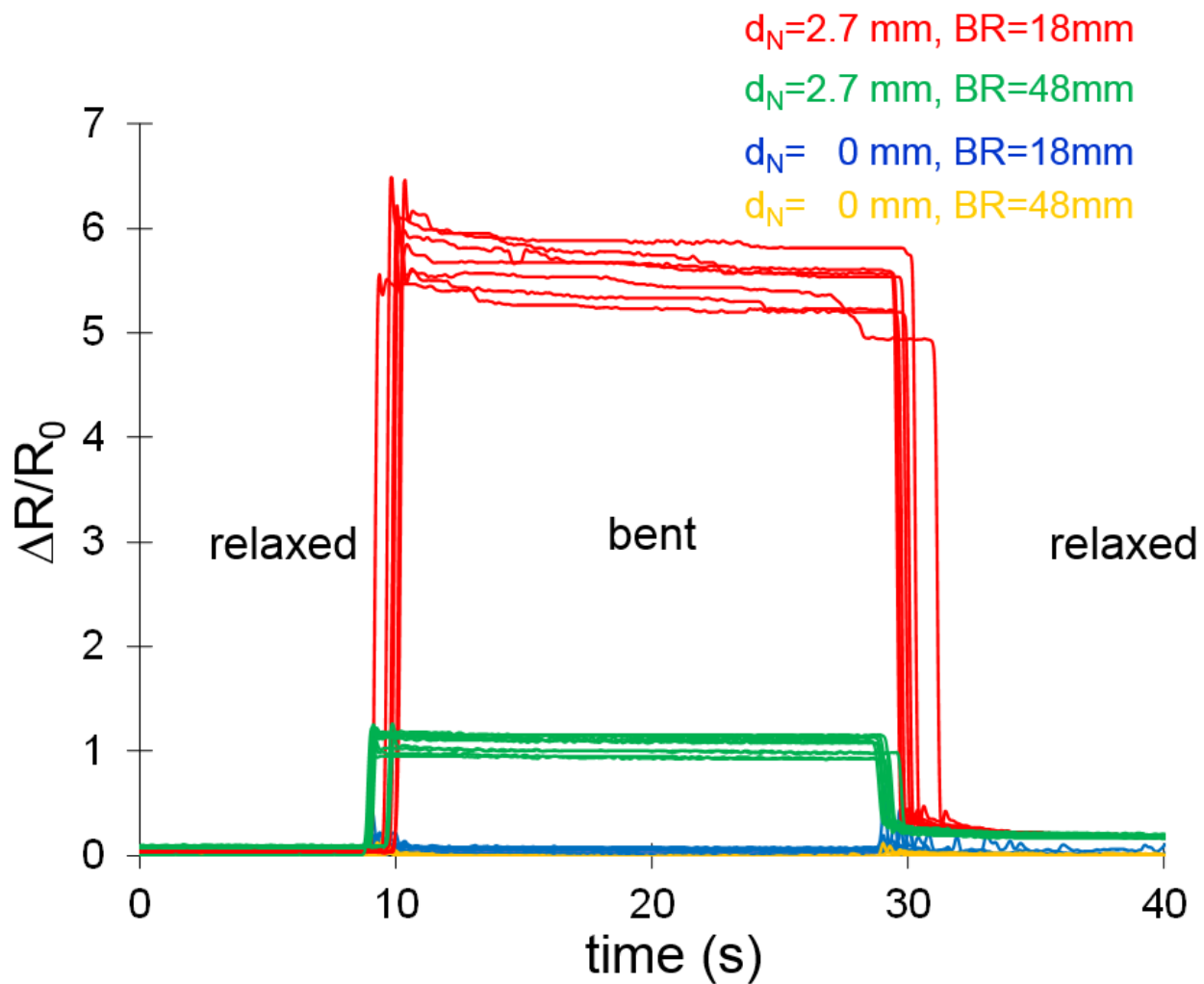
---

\* Authors to whom correspondences should be addressed:

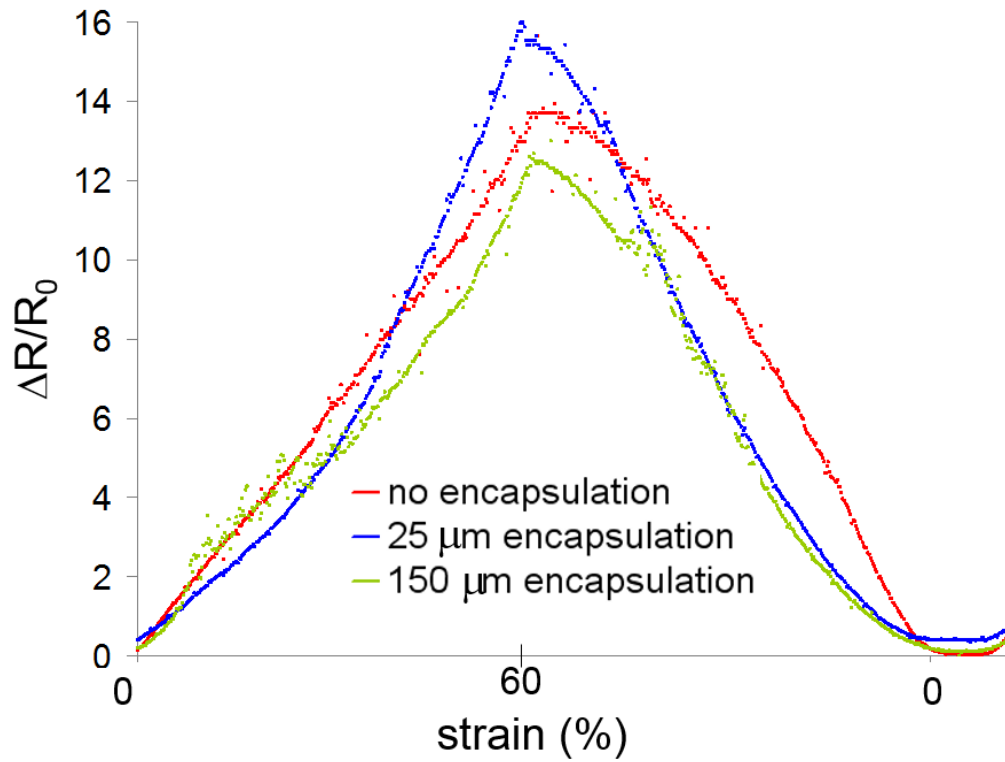
Fabrication and material properties, Email: [oliver.graudejus@asu.edu](mailto:oliver.graudejus@asu.edu)

Mechanics model, Email: [lit@umd.edu](mailto:lit@umd.edu)

## Supplementary Material



SFIG. 1. Comparison of the normalized change in resistance ( $\Delta R/R_0$ ) before (relaxed), during (bent), and after (relaxed) bending over several cycles; the resistance was measured for 10s with the sample being relaxed, for 20s with the sample being bent, and for 10s after relaxation.



SFIG. 2. Comparison of the normalized change in resistance ( $\Delta R/R_0$ ) vs. strain for encapsulated and not encapsulated gold conductors of 100  $\mu\text{m}$  width and 20 mm length.